Origin of Dynamical Properties in PMMA−C_{60} Nanocomposites

Jamie M. Kropka,[†] Karl W. Putz,[†] Victor Pryamitsyn,[†] Venkat Ganesan,[†] and Peter F. Green*[,‡]

Department of Chemical Engineering, The University of Texas at Austin, Austin, Texas 78712, and Department of Material Science and Engineering, Applied Physics, The University of Michigan, Ann Arbor, Michigan 48109

Received February 15, 2007; Revised Manuscript Received April 12, 2007

ABSTRACT: Poly(methyl methacrylate) (PMMA)−C_{60} nanocomposites, with compositions in the range $0 \leq \phi_{C60}{}^{wt} \leq 0.05$, are shown to exhibit systematic increases in dynamic shear moduli, in glass transition temperature (T_g), and in the longest relaxation time of the polymer (τ_R) with increasing fullerene concentration. We show that while the $\phi_{C60}{}^{wt}$ dependence of the plateau modulus can be reconciled with a conventional "filler" effect, the systematic increases in T_g and in τ_R are associated with specific interactions between the C_{60} and the polymer segments. In the melt, these segment−C_{60} interactions are proposed to reduce polymer segmental mobility in the vicinity of the particle surface and ultimately suppress polymer dynamics, as measured mechanically, in a manner consistent with an increase in the polymer segmental friction coefficient.

Introduction

The influence of particles on the viscoelastic properties of conventional polymer-based composites, i.e., polymers filled with particles that have dimensions on the order of microns or larger, can often be described solely in terms of the volume fraction of particles.[1] The success of such a "filler" effect model relies on the influence of specific interactions between polymer segments and particles being negligible. However, when particles possess dimensions on the order of nanometers, even small particle concentrations can lead to a breakdown of this "continuum-solvent" wisdom. These polymer nanocomposite (PNC) materials exhibit changes in glass transition temperatures (T_g)[2−7] and enhancements in viscoelastic properties[8−15] unprecedented in conventional composites.

The unique properties of PNCs are attributed to the high filler surface area-to-volume ratios, which result in significant interfacial areas of contact between the polymer and the particles. The large interfacial areas of contact enable a substantial fraction of polymer segments to interact directly with filler particles, even at low particle concentrations. In addition, interparticle distances can become comparable to the size of the polymer chains at low particle volume fractions in PNCs. Consequently, both chain confinement and polymer bridging between particles can occur and may also influence the properties of the PNC. For many applications, however, the precise manner in which the preceding features interplay and impact material properties remains to be clarified.

The rheological behavior of PNCs has attracted significant interest in recent years,[8−12,14−20] for both scientific and technological reasons. Apart from providing an assessment of processability, rheological measurements give insight into the connection between the molecular structure and dynamics of polymers. Experimentally, PNCs typically exhibit solidlike viscoelastic behavior at particle volume fractions much smaller than predicted for conventional composites.[8,11,14] Explanations for this phenomenon range from jamming of a highly anisotropic particulate phase[9,16,21] to the creation of a polymer-mediated particle network.[11,14] Simulations suggest that changes in monomer packing near the polymer−particle interface[19,22−27] lead to local segmental dynamics that differ from that of the homopolymer. In the case of attractive polymer−particle interactions, the dynamics and can be highly heterogeneous,[19] particularly at high loading fractions.[20] These dynamic heterogeneities, which arise due to the presence of nanofillers, have been suggested to underlie changes in the T_g and the viscosity observed in PNCs.[19,20,25,26] Additional experimental studies aimed at discerning the nature of the material heterogeneities would be useful to gain further insight into these observations.

In this paper we examine how nanoparticles influence the viscoelastic behavior of PMMA-based PNCs and probe the underlying mechanism(s) of the effect. To this end, the thermal and viscoelastic properties of a model PNC, narrow molecular weight distribution PMMA into which C_{60} fullerene particles are incorporated, are evaluated. The diameter of a C_{60} particle is ∼1 nm; so individually dispersed particles within the polymer matrix would therefore result in average interparticle distances comparable to the size of the polymer radius of gyration, $R_g \sim$ 14 nm, at volume fractions as low as 3×10^{-5}. Considering the similarities noted between PNCs and polymer thin films,[6,25] and noting that polymer thin film physical properties exhibit changes at film thicknesses greater than the polymer R_g,[28−33] the properties of PMMA should be expected to exhibit changes even at such low C_{60} fractions. Our investigations confirm that the addition of C_{60} to PMMA has ramifications beyond that of a conventional "filler" effect. Dynamic mechanical analysis (DMA) and differential scanning calorimetric (DSC) measurements both reveal a systematic increase in the T_g of the PNCs, and melt rheological measurements show that an increase in the polymer chain relaxation time accompanies the change in T_g. An assessment of the C_{60} dispersion within the polymer, considered together with recent computer simulation findings and incoherent neutron scattering experiments, suggests that transient interactions between the polymer chain segments and C_{60} aggregates are responsible for the reduction in dynamics.

Experimental Section

Materials. The PNCs were made via a solution dissolution−solvent evaporation method. The C_{60} (Alpha Aesar, 99+%) was

* To whom correspondence should be addressed.
[†] The University of Texas at Austin.
[‡] The University of Michigan.

10.1021/ma070407p CCC: $37.00
Published on Web 06/21/2007

added to toluene up to a concentration of 0.15 wt % and sonicated (Sonicor, SC-40) for 15 min to disperse the fullerenes into solution. PMMA (Pressure Chemical; $M_w = 254.7$ kg/mol, $M_w/M_n = 1.15$) was also dissolved in toluene, and the two solutions were mixed in proportion to create the appropriate nanocomposite concentration. The toluene was subsequently evaporated from the mixture at 348 K. Residual solvent was removed by drying the samples under high vacuum at 453 K for 15 h. The pure polymer and PNCs were compression-molded at 453 K into cylindrical and rectangular geometries for rheological and dynamic mechanical (DMA) testing, respectively.

Thermal Characterization. Differential scanning calorimetry measurements of the samples were taken on a DSC 7 (Perkin-Elmer) after residual solvent removal. Approximately 10 mg of material was heated from 298 to 473 K at a rate of 10 K/min in three cycles. Between each heat ramp, the material was annealed at 473 K for 5 min to erase previous thermal history and then cooled to 298 K at 100 K/min. The samples were then held at 298 K for 5 min to ensure temperature equilibration before beginning the next heat ramp. All measurements reported are of the second heating cycle, which was indistinguishable from the third heating cycle.

The dynamic mechanical behavior of the PNCs was examined using a Mark V DMTA (Rheometrics Scientific) in the single cantilever bending geometry. The experimental specimens were 30 mm long, 10 mm wide, and 1.1 mm thick. The samples were cooled to 123 K and held there for 10 min. Then the storage modulus (E'), loss modulus (E''), and loss tangent (tan δ) were analyzed at discrete frequencies of 0.1, 1, 10, and 50 Hz under a strain of 0.1% while the sample was heated from 123 to 483 K at a rate of 1 K/min. Strain sweeps verified that the reported measurements are within the linear viscoelastic regime. All samples are relaxed above their glass transition temperature just before testing.

Rheology. The melt viscoelastic properties of the PNCs were characterized using an advanced rheometric expansion system (ARES) rheometer (Rheometrics Scientific) equipped with 25 mm parallel plates under small-amplitude oscillatory shear strain. The average gap between the plates was 1 mm, and applied strains ranged from 5 to 10%. The frequency-dependent elastic ($G'(\omega)$) and loss ($G''(\omega)$) shear moduli were measured over a temperature range of 433−513 K by performing frequency, ω, sweeps from 0.1 to 100 rad/s. Strain sweeps verified that all reported measurements were within the linear viscoelastic regime. Master curves at 443 K were generated using Orchestrator (TA Instruments) software, which determined the horizontal shift factors (a_T) necessary to match the loss tangent (tan δ). Subsequent vertical shift factors (b_T) were required to superpose moduli due to changes in material density and variations in the separation gap with temperature.

Incoherent Neutron Scattering. Aluminum boats containing the polymer samples were placed in an annular, thin-walled aluminum cell that was mounted on the high flux backscattering spectrometer (HFBS)[34] on the NG2 beamline at the NIST Center for Neutron Research and cooled to 50 K under vacuum. The spectrometer operated in fixed window mode (stationary Doppler drive) with the elastic intensity recorded over a Q range of 0.25−1.75 Å^{-1}. The sample temperature was increased at a rate of 1 K/min to 525 K, and the elastic intensity was summed over intervals of 1 K. The HFBS energy resolution of ~0.8 μeV (fwhm) implies that dynamics on a time scale of 200 MHz (~1 ns) or slower contribute to elastic scattering, whereas faster processes contribute to inelastic scattering and a subsequent reduction in the elastic intensity.

The incoherent scattering cross section of hydrogen is ~20 times greater than the total scattering cross section of C or O and ~40 times larger than its own coherent scattering cross section. Hence, in the C_{60}−PMMA PNCs tested, the scattering is dominated by the incoherent scattering of the hydrogen atoms of the PMMA, and only the polymer dynamics is probed. The thickness of the sample films was ~0.05 mm to achieve >90% transmission and minimize multiple scattering. Raw data were normalized to monitor and to the intensity at the lowest measured temperature.

Dispersion. C_{60} dispersion within the PMMA matrix was characterized by transmission optical microscopy and transmission electron microscopy (TEM). Transmission optical micrographs of the cast films were recorded using an Axioskop 2 MAT (Zeiss) equipped with an Axiocam MRc5 CCD (Zeiss). For TEM analysis, portions of the dried films were cut into sections, ~50 nm in thickness, with a diamond knife using an Ultracut UCT ultramicrotome (Leica). Sections were placed on a 400 mesh copper grid and subsequently examined at an accelerating voltage of 80 kV using an EM 208 (Philips).

Results

Thermal Characterization. The dynamic mechanical moduli show no significant changes upon C_{60} addition for materials in the glassy or rubbery state (data not shown due to the absence of changes). This observation holds at all tested frequencies (0.1, 1, 10, and 50 Hz). All changes in the moduli are limited to the α-transition region and are due to changes in the onset of the transition. At the α-transition, a substantial drop in E' occurs while E'' exhibits a peak, which is indicative of viscous damping. When C_{60} is added to PMMA, the position of the peak exhibited by tan δ (E''/E') shifts to higher temperatures; the peak height and peak width, however, remain unchanged (Figure 1a). Similarly, the change in heat capacity of the materials associated with the glass transition (Figure 1b) shifts to higher temperatures upon particle addition, but the magnitude and breadth of the change remain unaltered. The frequency dependence of the α-transition is also unaffected by particle addition (Figure 1c).

The change in T_g from that of pure PMMA for the PMMA−C_{60} PNCs, as measured by both DSC and DMA, is shown in Figure 2. The DSC T_g was determined in the following manner: (1) straight lines were fit to the heat flow vs temperature curves before, during, and after the glass transition; (2) the points of intersection were taken as the onset and end point of the transition; and (3) the T_g was taken as one-half the change in heat capacity between the onset and end point of the transition. The DMA T_g was identified as the high-temperature peak position of tan δ plotted as a function of temperature. It is clear from Figure 2 that the T_g of the material increases with the addition of C_{60}.

Rheology. Dynamic rheological measurements were conducted to determine the effect of C_{60} on the dynamics and topology of the polymer melt. Master curves of the shear storage modulus and of the shear loss modulus at a reference temperature, $T_0 = 443$ K, are shown in Figure 3. It is evident from these data that the effect of C_{60} is to shift the storage and loss moduli to higher magnitudes and lower frequencies. The change in the magnitude of the storage modulus with ϕ_{C60}^{wt} is evaluated in terms of the plateau modulus, G_N^0, and the frequency shift in the moduli is evaluated in terms of the longest relaxation time of the polymer, τ_R, which is the reptation time for the highly entangled PMMA in our studies. An estimate of G_N^0 for the materials is obtained from the value of the elastic shear modulus at the point of maximum elasticity[35−37]

$$G_N^0 = [G'(\omega)]_{\min(\tan\delta)} \tag{1}$$

and is depicted as a function of ϕ_{C60}^{wt} in Figure 4. The longest relaxation time of the polymer is estimated as the crossover point of the storage and loss moduli at low frequency[38]

$$\tau_R = \left(\frac{2\pi}{a_T\omega}\right)_{G'=G''_{low\omega}} \tag{2}$$

and is plotted against ϕ_{C60}^{wt} in Figure 5. The two parameters G_N^0 and τ_R can be used to rescale the modulus and frequency axes, respectively, of the data in Figure 3 to account for strictly

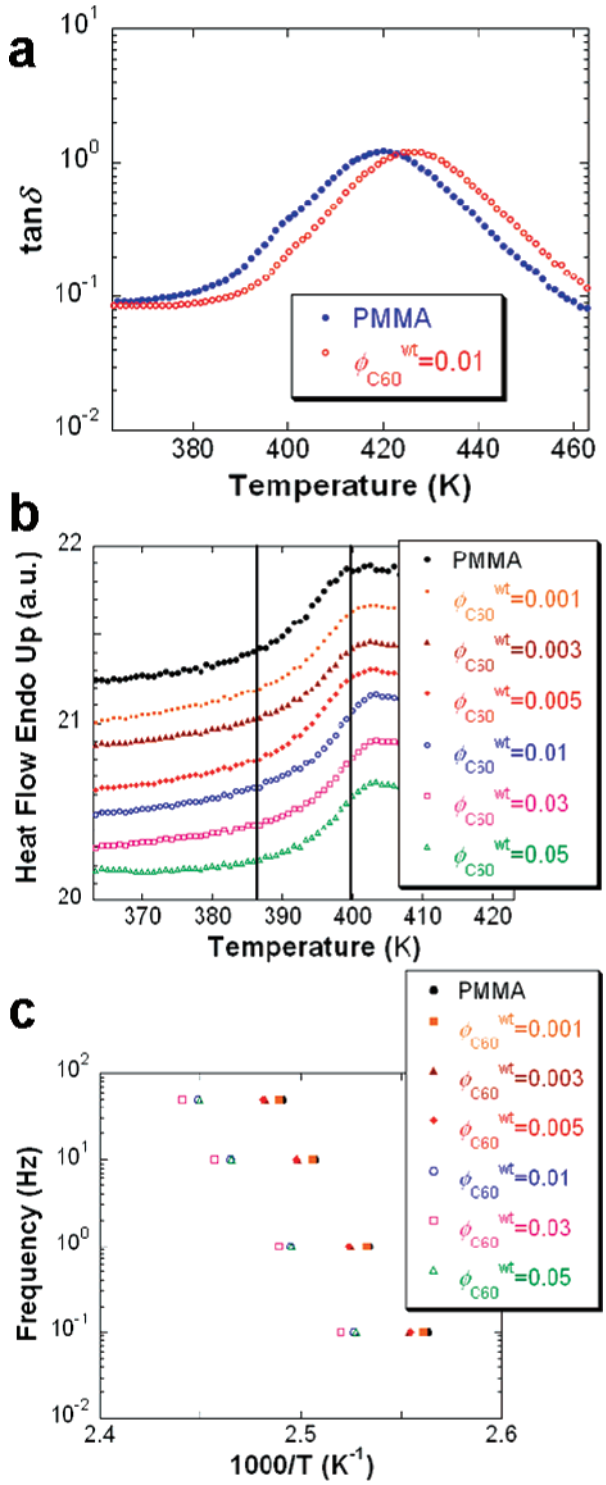

Figure 1. (a) Dynamic mechanical loss tangent, tan δ, as a function of temperature in the α-transition region for the pure polymer and PNC at a frequency of 10 Hz. For clarity, only the data for PMMA and the $\phi_{C60}^{wt} = 0.01$ PNC are shown. All other PNCs show similar behavior. (b) Differential scanning calorimetry thermograms for the pure polymer and PNCs. For clarity, the data have been shifted along the heat flow axis and only every fifth data point is shown. The vertical lines are drawn to aid in discerning the temperature shift of the transition. (c) Frequency dependence of the mechanical loss maximum associated with the α-transition for the pure polymer and PNCs.

vertical and horizontal shifts in the moduli. The rescaling results in the superposition of all data over the entire frequency range, as depicted in Figure 6.

The shift factors, a_T, necessary to construct the master curves of the viscoelastic data for each PNC are plotted as a function

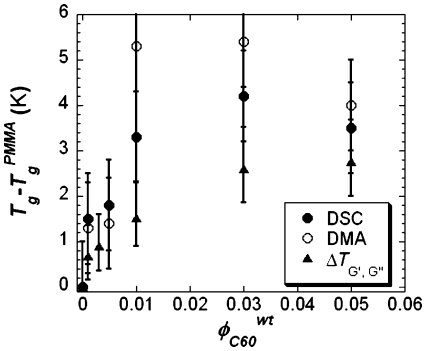

Figure 2. Change in the glass transition temperature from that of pure PMMA for the PMMA−C_{60} PNCs, $T_g - T_g^{PMMA}$, as measured by both DSC and DMA. The temperature shift necessary to superpose rheological moduli, $\Delta T_{G',G''}$, is also plotted for comparison. The error bars for the DSC measurements are associated with the range of values that can be obtained for reasonable choices of curve fits (as described in the text). For the DMA measurements, error bars are associated with the temperature difference between data points (i.e., the uncertainty with which the peak position is identified). The error bars for $\Delta T_{G',G''}$ are associated with both the measurement uncertainty of the crossover point of the storage and loss moduli (as described therein) and the range of WLF constants that gave a reasonable fit to the shift factor temperature dependence ($C_1^0 = 9.1-9.9$, $C_2^0 = 140-160$).

of temperature in Figure 7. The data from all samples superimpose onto a single curve that can be described by the Williams−Landel−Ferry (WLF) equation[39]

$$\log a_T = \frac{-C_1^0(T - T_0)}{C_2^0 + T - T_0} \tag{3}$$

with constants $C_1^0 = 9.5$ and $C_2^0 = 150$ at a reference temperature $T_0 = 443$ K. The ability to describe all data in Figure 7 by a single fit of eq 3 demonstrates the independence of both C_1^0 and C_2^0 on C_{60} concentration for the PNCs.

We conclude the rheological results and relate them to the thermal results by revealing the increase in τ_R with ϕ_{C60}^{wt}, shown in Figure 5, can be reconciled solely with the change in T_g of Figure 2. This relation is demonstrated by using eq 3 to calculate a temperature shift, $\Delta T_{G',G''}$, that is equivalent to the frequency shift, α, necessary to equate the longest relaxation times.

$$\alpha = \frac{\tau_R(\phi)}{\tau_R^{PMMA}} \tag{4}$$

$\Delta T_{G',G''}$ is plotted along with the experimentally determined T_g shift in Figure 2. The data show good agreement, supporting the notion that the changes in chain dynamics are determined by changes in the polymer matrix properties due to the influence of C_{60}.

Dispersion. Since nanoparticles are known to aggregate into clusters when dried from solution,[40] it is important to monitor particle dispersion in solution-fabricated materials. A visual observation of the polymer films that remained after solvent evaporation provided an initial assessment of C_{60} dispersion within the PMMA matrix. Prior to annealing, all films were translucent, with a purple hue. However, after annealing above T_g, samples of $\phi_{C60}^{wt} \geq 0.03$ became opaque. The opacity of the $\phi_{C60}^{wt} = 0.03$ and 0.05 samples is an indication of large particle agglomerates in the material, as nanoscopic fillers do not scatter light significantly.

Cross-sectional transmission electron microscopy (TEM) images of the PNCs (Figure 8) reveal that the C_{60} exists as nanoscopic agglomerates with diameters on the order of 20 nm

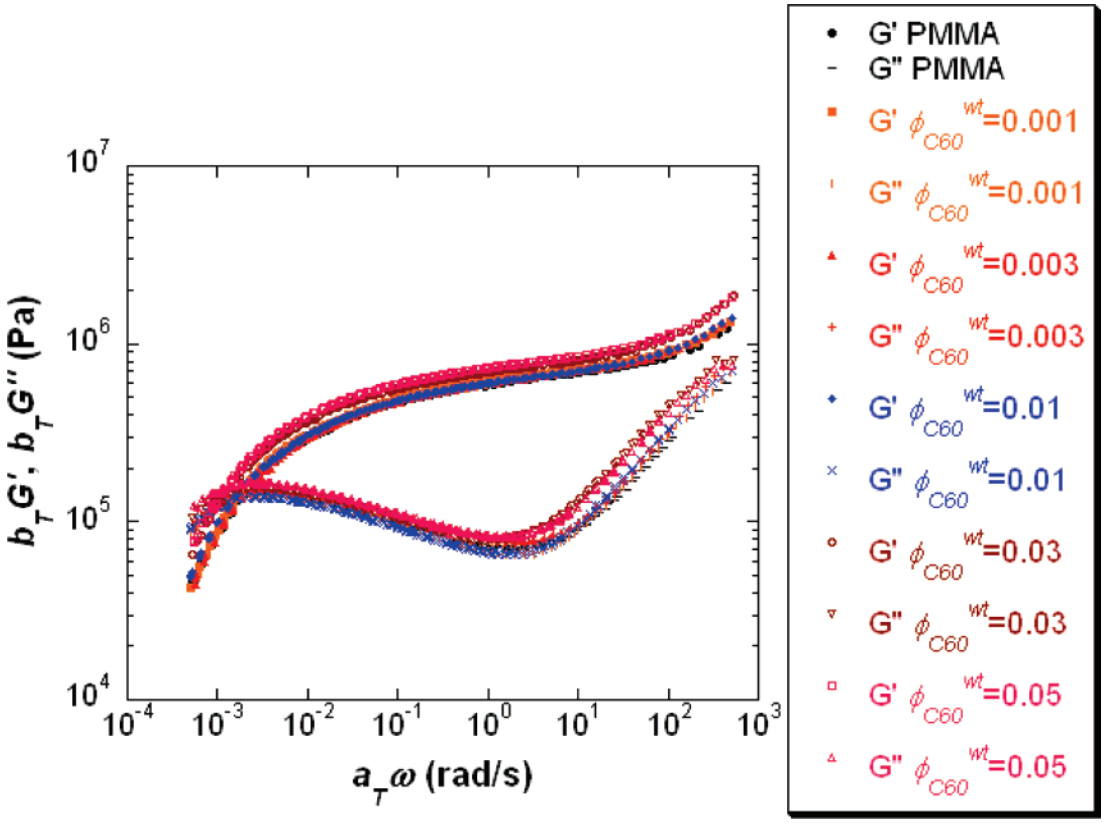

Figure 3. Frequency dependence of the dynamic shear moduli of the polymer and PNCs. Master curves were obtained by application of time−temperature superposition and were shifted to a reference temperature of 443 K.

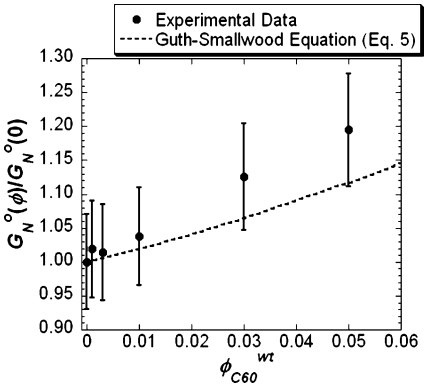

Figure 4. Ratio of the plateau moduli of the PNCs to that of pure PMMA as a function of C_{60} loading. The relation in eq 5 is plotted along with the data for comparison. The error bars for the plateau moduli are associated with the variability (∼5%) of equivalent measurements on material standards, and all replicate PNC measurements fell within this range.

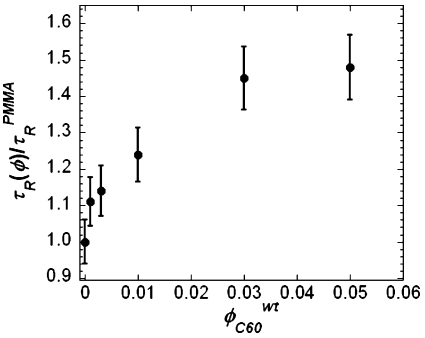

Figure 5. Ratio of the longest relaxation time for the PNCs to that of pure PMMA as a function of C_{60} loading. The error bars for the relaxation times are associated with the variability (∼3%) of equivalent measurements on material standards and all replicate PNC measurements fell within this range.

for $\phi_{C60}^{wt} < 0.01$. Also evident from Figure 8 is the invariance of agglomerate size and increase in the number density of agglomerates with increasing ϕ_{C60}^{wt} for $\phi_{C60}^{wt} < 0.01$. These observations suggest that although the fullerenes have not been individually dispersed, aggregates at these low concentrations can still be described as nanoparticles and have dimensions on the order of the polymer chain size, ∼10−20 nm.

At higher concentrations, $\phi_{C60}^{wt} \geq 0.01$, C_{60} agglomerates were detectable by both transmission optical microscopy and TEM. Figure 8 illustrates the coexistence of both nanoscopic and micron sized agglomerates at $\phi_{C60}^{wt} = 0.01$. From the TEM micrographs of the agglomerate structure at $\phi_{C60}^{wt} = 0.05$, it is evident that the morphology of the micron sized agglomerates is characterized by features on two additional length scales: (1) the large agglomerates consist of "bundles" of the nanoscopic aggregates that exist in the mixtures at low concentrations, and (2) crystal planes are evident within the nanoscopic aggregates. In fact, the relative abundance of the ordered nanometer agglomerates at high concentrations is likely the source of X-ray diffraction peaks observable by us (not shown) and by others[41] in these materials.

Discussion

As described in the Introduction, property enhancements exhibited by PNCs can result from two effects: (1) a "filler" effect that can be completely described by the volume fraction of particles and has been well characterized through studies of conventional composites and/or (2) changes in the polymer matrix properties due to specific interactions between the polymer chain segments and the nanoparticles. While the latter is relevant in many systems,[2−6,11,12,14,15] the specific mechanisms behind the influences are often not fully understood.

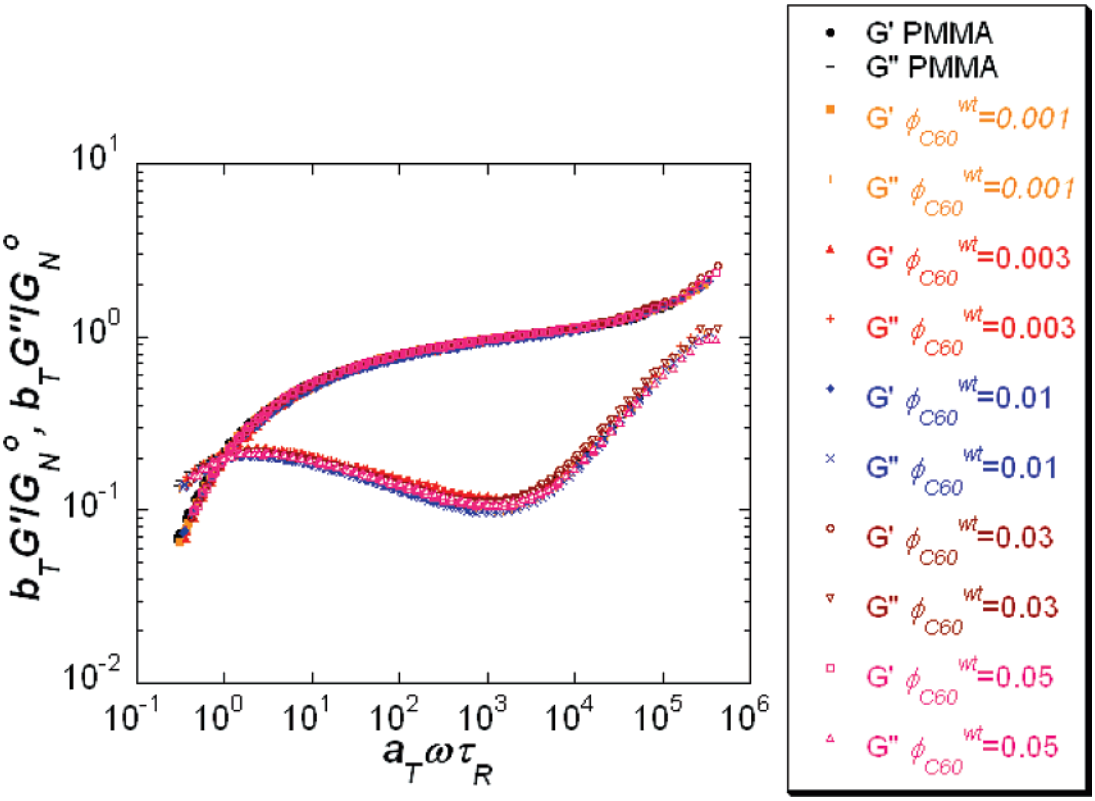

Figure 6. Superposition of the dynamic shear moduli by a rescaling of the axes as described in the text.

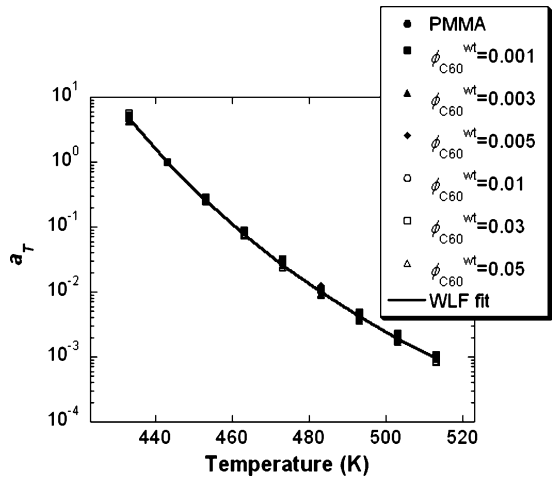

Figure 7. Frequency shift factors, a_T, used for the development of the master curves in Figure 3 as a function of temperature.

Simulations[19,22−27] suggest the presence of nanoparticles change local monomer packing and that such changes in structure can contribute to property enhancements. For instance, a decrease in fractional free volume associated with increased monomer packing density, due to the influence of nanoparticles, could account for the increase in T_g exhibited by the PMMA−C_{60} PNCs, assuming the glass transition is an iso-free volume process. The increase in T_g could, in turn, account for the slow down in melt dynamics. Another scenario might be that an increase in polymer entanglement density arises from increased monomer packing density or direct polymer−particle contacts. The resulting decrease in the number of monomers between entanglements, N_e, from such an effect could account for increases in the plateau modulus, $G_N^0 \sim N_e^{-1}$, and chain relaxation time, $\tau_R \sim N_e^{-1}$, exhibited by the PMMA−C_{60} PNCs. However, in what follows we will show that our experimental observations are not consistent with the foregoing interpretations. It will be shown that the increase in G_N^0 with C_{60} concentration is associated with the "filler" effect. In addition, we illustrate that the perturbing influence of the nanoparticles on the polymer matrix does not derive from polymer chain confinement or polymer bridging between particles. Instead, we argue that the increases in τ_R and T_g reflect the subtle influence of transient interactions between the fullerene surfaces and the PMMA chain segments.

Free Volume and Polymer Entanglement Density. As just described, changes in system free volume and/or polymer entanglement density, due to an influence of nanoparticles on polymer packing, could be responsible for changes in T_g, τ_R, and G_N^0 in PNCs. For instance, in PMMA−POSS PNCs, a WLF analysis enables a rationalization of the changes in system T_g in terms of changes in free volume with POSS concentration.[42] The rheological measurements of the PMMA−C_{60} PNCs, however, fail to resolve any such changes in structure. The WLF constants are independent of C_{60} concentration in these materials, which suggests that free volume changes cannot explain the trends exhibited in T_g.

An analysis of the breadth of the plateau region of the rheological data reveals that the PMMA entanglement density is independent of C_{60} concentration. The breadth of the plateau region is defined by the difference between τ_R and τ_e, the latter denoting the Rouse time of an entanglement strand. Since $\tau_R \sim N_e^{-1}$ and $\tau_e \sim N_e^2$, a change in N_e would result in a change in the breadth of the plateau region. However, Figure 6 illustrates the invariance of the breadth of the plateau region with C_{60} concentration; the data for the homopolymer and all PNCs superpose over the entire frequency range, which extends beyond the plateau region at both high and low frequencies, after rescaling to account for strictly horizontal and vertical shifts in the moduli. Since no change in the breadth of the plateau region occurs upon C_{60} addition, changes in the entanglement density cannot account for the observed changes in plateau

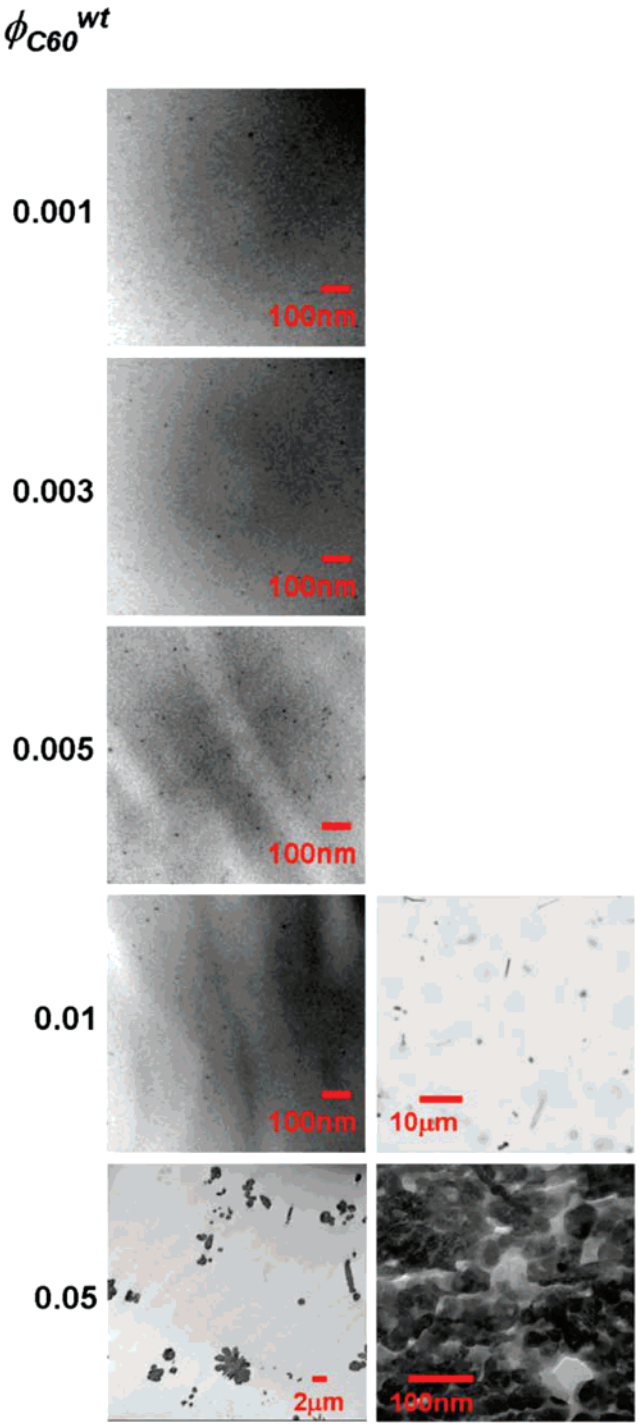

Figure 8. TEM and optical micrographs of the PMMA−C_{60} PNCs. The dark features are C_{60} agglomerates. At $\phi_{C60}^{wt} < 0.01$, C_{60} agglomerates are ~20 nm in diameter. At $\phi_{C60}^{wt} = 0.01$ nanoscale agglomerates coexist with micron sized agglomerates. The micron sized agglomerates at $\phi_{C60}^{wt} = 0.05$ consists of "bundles" of the nanoscale agglomerates that exist at low C_{60} concentrations, and these nanoscale agglomerates exhibit ordered packing of C_{60} particles.

modulus or polymer melt dynamics. These findings suggest the need for alternative explanations for the behavior of the PMMA−C_{60} PNCs, and the goal of the following discussion will be to identify the mechanisms behind the C_{60} influence on the properties of the PNCs.

The "Filler" Effect. We now examine the increase in melt plateau modulus with C_{60} concentration using a continuum theory which describes the effect of hard, noninteracting, spherical fillers on the moduli of polymers. The theory relates the modulus of the composite, $G_N^0(\phi^{vol})$, to that of the polymer, $G_N^0(0)$, by a filler volume fraction, ϕ^{vol}, dependent term.[43,44]

$$G_N^o(\phi^{vol}) = G_N^0(0)[1 + 2.5\phi^{vol} + 14.1(\phi^{vol})^2] \qquad (5)$$

While eq 5, often referred to as the Guth−Smallwood equation, under predicts the compositional dependence of the modulus depicted in Figure 4, the small discrepancy can be accounted for by a number of factors. The TEM images in Figure 8 show that the micron sized agglomerates which exist for $\phi_{C60}^{wt} > 0.01$ are anisotropic and contain voids (the light areas within the C_{60} agglomerates). The anisotropy of the particles alone contribute to deviations from eq 5,[43] and the voids within the agglomerate structure lead to larger effective volume fractions of the filler. Both effects tend to increase the magnitude of G_N^0 beyond the theoretical predictions. Although it would be difficult to quantify the deviations from eq 5 due to these effects, we argue that they account for the discrepancies in Figure 4 and attribute the origin of the increase of G_N^0 with C_{60} concentration to the "filler" effect.

Factors of Influence on PMMA Matrix Properties. Our results show that C_{60} perturbs the polymer matrix in such a manner as to increase the T_g and polymer chain relaxation time. The confinement of chains between filler particles, polymer bridging between particles, and polymer−particle interfacial interactions may all contribute toward the influence that nanoparticles have on the properties of polymers. We now examine the relative role these factors play in shaping the properties exhibited by the PMMA−C_{60} PNCs.

Chain confinement effects are expected be significant when interparticle distances become smaller than the size of the polymer, ~$2R_g$. An estimate of the C_{60} interparticle distance, h, using the relation

$$\frac{h}{D} = \left(\frac{\phi_m^{vol}}{\phi^{vol}}\right)^{1/3} - 1, \quad \phi_m^{vol} = 0.638 \qquad (6)$$

where D is the particle diameter and ϕ_m^{vol} is the maximum random packing volume fraction, predicts that $h \sim 2R_g$ for $\phi_{C60}^{vol} \sim 2.6 \times 10^{-5}$ ($\phi_{C60}^{wt} \sim 4.5 \times 10^{-5}$). This calculation is based on the assumption that the C_{60} particles are individually dispersed and suggests that the polymer molecules in the PMMA−C_{60} PNCs evaluated, $\phi_{C60}^{wt} \geq 0.001$, are highly confined between particles. However, the TEM images in Figure 8 reveal that much of the C_{60} exists as aggregates. For $\phi_{C60}^{wt} < 0.01$, the average size of the aggregates is on order of 20 nm in diameter; for higher C_{60} concentrations the dimensions of the aggregates reach the order of microns. On the basis of eq 6, the distance between these aggregates is greater than the size of the polymer, $h > 2R_g$, at all C_{60} concentrations. This conclusion is consistent with the observation of interparticle distances in the micrographs of Figure 8. Therefore, confinement of the polymer chains between particles does not contribute to the observed changes in T_g and chain dynamics for the PMMA−C_{60} PNCs.

Polymer chain bridging between particles also requires that the size of the polymer chain exceed the interparticle distances. However, we have already established that $h > 2R_g$ in the PMMA−C_{60} mixtures, so any mechanism based solely on particle bridging would not be significant. Moreover, the lack of formation of a percolated filler network mediated by polymer chains, associated with polymer bridging between particles, is also evident from the melt dynamic shear moduli in Figure 3.

Such a network restrains long-range motions of polymer chains; the liquidlike terminal behavior associated with homopolymers at long time scales transitions to solidlike behavior.[9,11,14,20] An example of this phenomenon was observed by Du et al.[14] in PMMA-single-walled carbon nanotube (SWNT) PNCs. The dynamic viscoelastic moduli of the PMMA−SWNT PNCs exhibit a weak low-frequency dependence for SWNT loadings higher than 0.2 wt %, thereby revealing the restraint of the long-range polymer chain motions at these SWNT concentrations. However, the PMMA−C_{60} materials exhibit homopolymer-like terminal flow behavior, $G' \sim \omega^2$ and $G'' \sim \omega$, at all C_{60} loadings; only a shift in the onset of terminal flow to lower frequencies (Figure 3) occurs. This frequency shift in the rheological behavior with C_{60} addition is present throughout the entire frequency range, suggesting that polymer chain dynamics are affected equally on all length scales. This behavior is in contrast to that of a percolated network, where influence would primarily be in the terminal flow regime. Hence, both interparticle distances that exceed polymer chain size and the terminal flow behavior of the materials indicate that polymer bridging between particles is not the contributing influence to the changes in T_g and chain dynamics observed for the PMMA−C_{60} PNCs.

The absence of polymer chain confinement and polymer bridging between particles in the PMMA−C_{60} PNCs leaves interfacial interactions to account for the observed changes in PMMA matrix properties. This finding, in conjunction with the observations of C_{60} agglomerate size as a function of $\phi_{C60}{}^{wt}$ (Figure 8), makes the origin of the plateau of T_g and of τ_R at $\phi_{C60}{}^{wt} > 0.01$ (observed in Figures 2 and 5, respectively) apparent. The formation of large particle agglomerates at the higher concentrations prevents the growth of polymer−particle interfacial area of contact and hence inhibits the influence of the particles on the polymer dynamics from growing with further increases in C_{60} concentration. We now turn our attention to the manner by which interfacial interactions exert influence on the bulk behavior of the PMMA−C_{60} PNCs.

Role of Transient Interactions at Interfacial Contact. There is reasonable insight into ways that interfacial interactions influence the properties of polymers, particularly from measurements of the glass transition temperature of thin polymer films[28−33,45−48] and of PNCs.[2−7] In PNCs, particles are generally described to influence the glass transition of the material in one of two manners. The first is a relatively long-ranged gradient in T_g, extending tens of nanometers from the interface, that influences the average T_g of the material.[6] The second is a more localized effect denoted by marked changes in polymer dynamics at direct interfacial contact with the particles, i.e., "bound" polymer, while, at the same time, homopolymer-like dynamics are exhibited by chains away from the particle surface.[2,3,49] For the PMMA−C_{60} system, the invariance of the tan δ α-relaxation peak height and peak width with filler concentration (Figure 1a) is not consistent with either of the foregoing descriptions. A long-ranged gradient in the polymer T_g within the interfacial region would be anticipated to produce a broader distribution of polymer relaxation times compared to the homopolymer and hence broaden the width of the α-transition peak for the PNCs relative to the homopolymer. A marked change in dynamics at interfacial contact would be anticipated to shift the relaxation of a fraction of polymer segments outside the spectrum of the homopolymer α-transition peak and hence reduce the height of the α-transition peak for the PNCs relative to the homopolymer. The absence of either effect suggests that the C_{60} particles slow the α-relaxation dynamics uniformly throughout the bulk of the PNC.

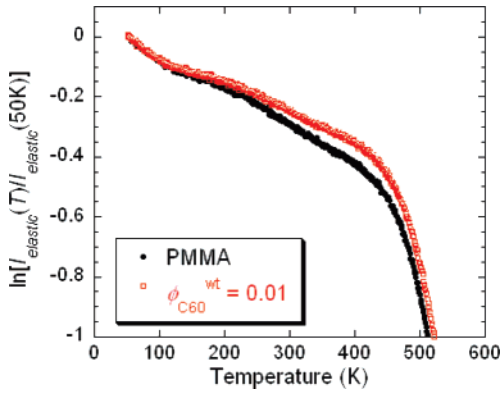

Figure 9. Decrease in the elastic scattering intensity, summed over all Q, as a function of temperature for PMMA and the $\phi_{C60}{}^{wt} = 0.01$ PNC.

Simulations[19,20,25,26] indicate that local dynamic heterogeneities in PNC melts, associated with polymer−particle interfacial interactions, can lead to a change in the macroscopic properties of the polymer. These simulations suggest that weakly attractive polymer−particle interactions lead to transient immobilization of polymer segments at the surfaces of particles; the duration of the immobilization persists on time scales, τ_{ps}, that are much shorter than the longest relaxation time, τ_R, of a polymer chain, $\tau_{ps} \ll \tau_R$. Consequently, a large fraction of polymer segments experience such transient interactions throughout the duration τ_R, and this induces a homogeneous slowdown of dynamics on the time scale of τ_R. The effect is tantamount to an increase in the effective friction experienced by a chain. Higher particle concentrations lead to larger polymer−particle interfacial areas of interaction (assuming the particles do not aggregate appreciably) and enhance the effect on dynamics. The work of Pryamitsyn et al.[20] describes this type of behavior at low concentrations of a spherical filler in PNCs with weakly attractive polymer−particle interactions; such as mechanism is also commensurate with our experimental observations of τ_R as described below.

Evidence of the immobilization of polymer chain segments at the surface of the C_{60} particles can be discerned from incoherent neutron scattering (INS) measurements. Figure 9 reveals an increase of the elastic scattering intensity for the $\phi_{C60}{}^{wt} = 0.01$ PNC relative to that of pure PMMA, indicating a decrease in atomic motions for the PNC relative to the homopolymer. Further, as will be described in detail in a future work, quasi-elastic neutron scattering measurements of the same systems, above T_g, reveal that the PNC exhibits a broader distribution of polymer relaxation times relative to the homopolymer. Hence, the increased elastic intensity for the PNC melt is attributed to motional restriction of polymer segments at the polymer−particle interfaces on the nanosecond time scale of the INS measurements, while all other polymer segments retain homopolymer-like dynamics on this time scale. However, in contrast to this dynamic heterogeneity observed in the INS measurements, mechanical measurements suggest that the effect of C_{60} on polymer melt dynamics may be described in terms of a homogeneous increase in the local friction factor throughout the bulk of the material. Observations that support this latter suggestion include the invariance of the shape of the PNC mechanical α-relaxation peak from that of pure PMMA (Figure 1a), the invariance of the temperature dependence of the PNC mechanical α-relaxation time from that of pure PMMA (Figure 1c), the invariance of the shape of the low-frequency peak in the PNC melt loss modulus from that of pure PMMA (Figure 6), and the frequency shift in the rheological moduli over the

entire frequency range of the measurements (Figure 3). The picture that emerges from these findings is that the heterogeneous PNC melt dynamics at the nanosecond time scale of the INS measurements result in a homogeneous slowing of the bulk dynamics measured mechanically. The homogeneous effect on polymer dynamics on the time scale of τ_R can be attributed to the mechanism described above for the simulations. We also propose an alternative mechanism to describe the α-relaxation behavior as follows.

Motions associated with the mechanical α-relaxation peak are localized cooperative motions, and this begs the question as to how segments greater than 10 nm away from the particle surface would experience an equivalent reduction in dynamics as segments in direct contact with the surface. One way to interpret the shift in the α-relaxation dynamics of the PMMA−C_{60} PNCs may lie in the ideas presented by Long and Lequeux,[50] where a mechanism for the glass transition is proposed. In their work, Long and Lequeux regard system dynamics to be strongly heterogeneous, characterized by the presence of both slow domains and fast domains that result from thermally induced density fluctuations. They interpret the glass transition as a dynamical effect that results from the percolation of slow domains (which have a lifetime comparable to that of the α-relaxation, ∼10−100 s) throughout the system. In our case, the PMMA−C_{60} interactions enhance the fraction of slow domains in the PNC relative to the homopolymer. Consequently, the percolation of slow domains occurs at a higher temperature in the PNC than in the homopolymer, and hence the PNC T_g and associated α-relaxation motions are shifted to higher temperatures. Thus, in this framework, it is not necessary for the particles to influence all polymer segments uniformly to obtain a shift in the α-relaxation dynamics as found in the DMA measurements of the PMMA−C_{60} PNCs. Only a shift in the temperature at which percolation occurs is necessary, and this can be accomplished via the polymer−particle interfacial interactions described heretofore.

Conclusions

We have shown how small concentrations of C_{60} in PMMA increase the melt shear moduli, the glass transition temperature, and the longest relaxation time of the polymer. The increases in shear plateau modulus are associated with a so-called conventional "filler" effect; however, the increases in T_g and τ_R are associated with a change in polymer matrix properties that reveals a breakdown of polymer "continuum solvent" behavior in the PNCs. Since the mechanical measurements resolve a uniform change in polymer dynamics with nanoparticle addition, it is tempting to attribute the decrease in dynamics to a decrease in free volume or an increase in polymer entanglement density associated tighter segmental packing due to the influence of the nanoparticles. However, no such structural changes are discerned; the increases in τ_R are shown to result from transient immobilization of polymer segments at the particle surface that lead to an increase in the effective friction experienced by the chains. An increase in the fraction of slowly relaxing polymer domains due to the PMMA−C_{60} interfacial interactions is also proposed to account for the shift in T_g and the associated α-relaxation dynamics by increasing the temperature at which percolation of the slow domains occurs. The development of such dynamical heterogeneities upon the addition of nanoparticles is supported by simulations and by INS measurements that probe polymer segmental motions on a nanosecond time scale. Higher particle concentrations lead to more polymer−particle interfacial area and increase the magnitude of the observed effects. However, the growth of polymer−particle interfacial area is inhibited when increased particle concentration leads to the formation of larger particle aggregates, and the magnitude of the effect on dynamics in this scenario is limited.

Acknowledgment. This work was funded by the National Science Foundation (DMR 0601890) and utilized facilities supported in part by the National Science Foundation under Agreement DMR-0454672. We acknowledge the support of the National Institute of Standards and Technology, U.S. Department of Commerce, in providing the neutron facilities used in this work. J.M.K. thanks Victoria Garcia-Sakai for her help with the HFBS instrument. V.G. is grateful for partial support from the Welsh Foundation and NSF Grant CTS 0347381.

References and Notes

(1) Russel, W. B.; Saville, D. A.; Schowalter, W. R. *Colliodal Dispersions*; Cambridge University Press: New York, 1989.
(2) Tsagaropoulos, G.; Eisenburg, A. *Macromolecules* **1995**, *28*, 396−398.
(3) Tsagaropoulos, G.; Eisenberg, A. *Macromolecules* **1995**, *28*, 6067−6077.
(4) Becker, C.; Krug, H.; Schmidt, H. *Mater. Res. Soc. Symp. Proc.* **1996**, *435*, 237−242.
(5) Ash, B. J.; Siegel, R. W.; Schadler, L. S. *J. Polym. Sci., Part B: Polym. Phys.* **2004**, *42*, 4371−4383.
(6) Bansal, A.; Yang, H.; Li, C.; Cho, K.; Benicewicz, B. C.; Kumar, S. K.; Schadler, L. S. *Nat. Mater.* **2005**, *4*, 693−698.
(7) Rittigstein, P.; Torkelson, J. M. *J. Polym. Sci., Part B: Polym. Phys.* **2006**, *44*, 2935−2943.
(8) Krishnamoorti, R.; Vaia, R. A.; Giannelis, E. P. *Chem. Mater.* **1996**, *8*, 1728−1734.
(9) Krishnamoorti, R.; Giannelis, E. P. *Macromolecules* **1997**, *30*, 4097−4102.
(10) Yurekli, K.; Krishnamoorti, R.; Tse, M. F.; McElrath, K. O.; Tsou, A. H.; Wang, H. C. *J. Polym. Sci., Part B: Polym. Phys.* **2000**, *39*, 256−275.
(11) Zhang, Q.; Archer, L. A. *Langmuir* **2002**, *18*, 10435−10442.
(12) Mackay, M. E.; Dao, T. T.; Tuteja, A.; Ho, D. L.; Van Horn, B.; Kim, H.-C.; Hawker, C. J. *Nat. Mater.* **2003**, *2*, 762−766.
(13) Putz, K. W.; Mitchell, C. A.; Krishnamoorti, R.; Green, P. F. *J. Polym. Sci., Part B: Polym. Phys.* **2004**, *42*, 2286−2293.
(14) Du, F.; Scogna, R. C.; Zhou, W.; Brand, S.; Fischer, J. E.; Winey, K. I. *Macromolecules* **2004**, *37*, 9048−9055.
(15) Tuteja, A.; Mackay, M. E.; Hawker, C. J.; Van Horn, B. *Macromolecules* **2005**, *38*, 8000−8011.
(16) Galgali, G.; Ramesh, C.; Lele, A. *Macromolecules* **2001**, *34*, 852−858.
(17) Solomon, M. J.; Almusallam, A. S.; Seefeldt, K. F.; Somwangthanaroj, A.; Varadan, P. *Macromolecules* **2001**, *34*, 1864−1872.
(18) Potschke, P.; Fornes, T. D.; Paul, D. R. *Polymer* **2002**, *43*, 3247−3255.
(19) Smith, G. D.; Bedrov, D.; Li, L.; Byutner, O. *J. Chem. Phys.* **2002**, *117*, 9478−9489.
(20) Pryamitsyn, V.; Ganesan, V. *Macromolecules* **2006**, *39*, 844−856.
(21) Krishnamoorti, R.; Yurekli, K. *Curr. Opin. Colloid Interface Sci.* **2001**, *6*, 464−470.
(22) Desai, T.; Keblinski, P.; Kumar, S. K. *J. Chem. Phys.* **2005**, *122*, 134910/134911−134910/134918.
(23) Vacatello, M. *Macromolecules* **2001**, *34*, 1946−1952.
(24) Vacatello, M. *Macromol. Theory Simul.* **2002**, *11*, 757−765.
(25) Starr, F. W.; Schroder, T. B.; Glotzer, S. C. *Phys. Rev. E* **2001**, *64*, 021802.
(26) Starr, F. W.; Schroder, T. B.; Glotzer, S. C. *Macromolecules* **2002**, *35*, 4481−4492.
(27) Brown, D.; Mele, P.; Marceau, S.; Alberola, N. D. *Macromolecules* **2003**, *36*, 1395−1406.
(28) Keddie, J. L.; Jones, R. A. L.; Cory, R. A. *Europhys. Lett.* **1994**, *27*, 59−64.
(29) van Zanten, J. H.; Wallace, W. E.; Wu, W.-l. *Phys. Rev. E* **1996**, *53*, R2053−R2056.
(30) Ellison, C. J.; Torkelson, J. M. *Nat. Mater.* **2003**, *2*, 695−700.
(31) Pham, J. Q.; Green, P. F. *Macromolecules* **2003**, *36*, 1665−1669.
(32) Soles, C. L.; Douglas, J. F.; Wu, W.-L. *J. Polym. Sci., Part B: Polym. Phys.* **2004**, *42*, 3218−3234.
(33) Besancon, B. M.; Soles, C. L.; Green, P. F. *Phys. Rev. Lett.* **2006**, *97*, 057801.
(34) Meyer, A.; Dimeo, R. M.; Gehring, P. M.; Neumann, D. A. *Rev. Sci. Instrum.* **2003**, *74*, 2759−2777.

(35) Wu, S. *J. Polym. Sci., Part B: Polym. Phys.* **1989**, *27*, 723−741.
(36) Lomellini, P.; Lavagnini, L. *Rheol. Acta* **1992**, *31*, 175−182.
(37) Fuchs, K.; Friedrich, C.; Weese, J. *Macromolecules* **1996**, *29*, 5893−5901.
(38) Rubinstein, M.; Colby, R. H. *Polymer Physics*; Oxford University Press: New York, 2003.
(39) Ferry, J. D. *Viscoelastic Properties of Polymers*, 3rd ed.; Wiley: New York, 1980.
(40) Mackay, M. E.; Tuteja, A.; Duxbury, P. M.; Hawker, C. J.; Van Horn, B.; Guan, Z.; Chen, G.; Krishnan, R. S. *Science (Washington, DC, U.S.)* **2006**, *311*, 1740−1743.
(41) Chen, G.; Ma, G. *Appl. Phys. Lett.* **1998**, *72*, 3294−3296.
(42) Kopesky, E. T.; Haddad, T. S.; McKinley, G. H.; Cohen, R. E. *Polymer* **2005**, *46*, 4743−4752.
(43) Guth, E. *J. Appl. Phys.* **1945**, *16*, 20−25.
(44) Smallwood, H. M. *J. Appl. Phys.* **1944**, *15*, 758−766.
(45) Keddie, J. L.; Jones, R. A. L.; Cory, R. A. *Faraday Discuss.* **1995**, *98*, 219−230.
(46) Forrest, J. A.; Dalnoki-Veress, K.; Stevens, J. R.; Dutcher, J. R. *Phys. Rev. Lett.* **1996**, *77*, 2002−2005.
(47) Fryer, D. S.; Peters, R. D.; Kim, E. J.; Tomaszewski, J. E.; de Pablo, J. J.; Nealey, P. F.; White, C. C.; Wu, W.-l. *Macromolecules* **2001**, *34*, 5627−5634.
(48) Ellison, C. J.; Kim, S. D.; Hall, D. B.; Torkelson, J. M. *Eur. Phys. J. E* **2002**, *8*, 155−166.
(49) Berriot, J.; Montes, H.; Lequeux, F.; Long, D.; Sotta, P. *Europhys. Lett.* **2003**, *64*, 50−56.
(50) Long, D.; Lequeux, F. *Eur. Phys. J. E* **2001**, *4*, 371−387.

MA070407P